The Astrophysical Journal Letters, 734:L12 (7pp), 2011 June 10 doi:10.1088/2041-8205/734/1/L12

HerMES: LYMAN BREAK GALAXIES INDIVIDUALLY DETECTED AT $0.7 \leqslant z \leqslant 2.0$ IN GOODS-N WITH *HERSCHEL*/SPIRE

D. Burgarella[1], S. Heinis[1], G. Magdis[2], R. Auld[3], A. Blain[4], J. Bock[5,6], D. Brisbin[7], V. Buat[1], P. Chanial[8], D. L. Clements[8], A. Cooray[5,9], S. Eales[3], A. Franceschini[10], E. Giovannoli[1], J. Glenn[11], E. A. González Solares[12], M. Griffin[3], H. S. Hwang[2], O. Ilbert[1], L. Marchetti[10], A. M. J. Mortier[8], S. J. Oliver[13], M. J. Page[14], A. Papageorgiou[3], C. P. Pearson[15,16], I. Pérez-Fournon[17,18], M. Pohlen[3], J. I. Rawlings[14], G. Raymond[3], D. Rigopoulou[19,20], G. Rodighiero[10], I. G. Roseboom[13], M. Rowan-Robinson[8], Douglas Scott[21], N. Seymour[14], A. J. Smith[13], M. Symeonidis[14], K. E. Tugwell[14], M. Vaccari[10], J. D. Vieira[5], M. Viero[5], L. Vigroux[22], L. Wang[13], and G. Wright[23]

[1] Laboratoire d'Astrophysique de Marseille, OAMP, Université Aix-Marseille, CNRS, 38 rue Frédéric Joliot-Curie, 13388 Marseille Cedex 13, France; denis.burgarella@oamp.fr, sebastien.heinis@oamp.fr

[2] Laboratoire AIM-Paris-Saclay, CEA/DSM/Irfu-CNRS-Université Paris Diderot, CE-Saclay, pt courrier 131, F-91191 Gif-sur-Yvette, France

[3] Cardiff School of Physics and Astronomy, Cardiff University, Queens Buildings, The Parade, Cardiff CF24 3AA, UK

[4] Institute for Astronomy, University of Edinburgh, Royal Observatory, Blackford Hill, Edinburgh EH9 3HJ, UK

[5] California Institute of Technology, 1200 East California Boulevard, Pasadena, CA 91125, USA

[6] Jet Propulsion Laboratory, 4800 Oak Grove Drive, Pasadena, CA 91109, USA

[7] Space Science Building, Cornell University, Ithaca, NY 14853-6801, USA

[8] Astrophysics Group, Imperial College London, Blackett Laboratory, Prince Consort Road, London SW7 2AZ, UK

[9] Department of Physics & Astronomy, University of California, Irvine, CA 92697, USA

[10] Dipartimento di Astronomia, Università di Padova, vicolo Osservatorio, 3, 35122 Padova, Italy

[11] Department of Astrophysical and Planetary Sciences, CASA 389-UCB, University of Colorado, Boulder, CO 80309, USA

[12] Institute of Astronomy, University of Cambridge, Madingley Road, Cambridge CB3 0HA, UK

[13] Astronomy Centre, Department of Physics & Astronomy, University of Sussex, Brighton BN1 9QH, UK

[14] Mullard Space Science Laboratory, University College London, Holmbury St. Mary, Dorking, Surrey RH5 6NT, UK

[15] RAL Space, Rutherford Appleton Laboratory, Chilton, Didcot, Oxfordshire OX11 0QX, UK

[16] Institute for Space Imaging Science, University of Lethbridge, Lethbridge, Alberta T1K 3M4, Canada

[17] Instituto de Astrofísica de Canarias (IAC), E-38200 La Laguna, Tenerife, Spain

[18] Departamento de Astrofísica, Universidad de La Laguna (ULL), E-38205 La Laguna, Tenerife, Spain

[19] Space Science & Technology Department, Rutherford Appleton Laboratory, Chilton, Didcot, Oxfordshire OX11 0QX, UK

[20] Oxford Astrophysics, Department of Physics Oxford University, Keble Road, Oxford OX1 3RH, UK

[21] Department of Physics & Astronomy, University of British Columbia, 6224 Agricultural Road, Vancouver, BC V6T 1Z1, Canada

[22] Institut d'Astrophysique de Paris, UMR 7095, CNRS, UPMC Univ. Paris 06, 98bis boulevard Arago, F-75014 Paris, France

[23] UK Astronomy Technology Centre, Royal Observatory, Blackford Hill, Edinburgh EH9 3HJ, UK

Received 2011 January 31; accepted 2011 April 28; published 2011 May 19

ABSTRACT

As part of the *Herschel* Multi-tiered Extragalactic Survey we have investigated the rest-frame far-infrared (FIR) properties of a sample of more than 4800 Lyman break galaxies (LBGs) in the Great Observatories Origins Deep Survey North field. Most LBGs are not detected individually, but we do detect a sub-sample of 12 objects at $0.7 < z < 1.6$ and one object at $z = 2.0$. The ones detected by *Herschel* SPIRE have redder observed NUV $- U$ and $U - R$ colors than the others, while the undetected ones have colors consistent with average LBGs at $z > 2.5$. The UV-to-FIR spectral energy distributions of the objects detected in the rest-frame FIR are investigated using the code CIGALE to estimate physical parameters. We find that LBGs detected by SPIRE are high-mass, luminous infrared galaxies. It appears that LBGs are located in a triangle-shaped region in the $A_{\rm FUV}$ versus $\log L_{\rm FUV} = 0$ diagram limited by $A_{\rm FUV} = 0$ at the bottom and by a diagonal following the temporal evolution of the most massive galaxies from the bottom right to the top left of the diagram. This upper envelop can be used as upper limits for the UV dust attenuation as a function of $L_{\rm FUV}$. The limits of this region are well explained using a closed-box model, where the chemical evolution of galaxies produces metals, which in turn lead to higher dust attenuation when the galaxies age.

Key words: galaxies: evolution – galaxies: formation – galaxies: high-redshift – infrared: galaxies – ultraviolet: galaxies

Online-only material: color figures

1. INTRODUCTION

The safest way to estimate the total star formation rates (SFRs) of galaxies is to consider the energy budget involving far-ultraviolet (FUV) and far-infrared (FIR) measurements (e.g., Buat & Xu 1996). Because only a small number of individual Lyman break galaxies (LBGs) have been detected in the FIR/submillimeter range (e.g., Chapman et al. 2000; Chapman & Casey 2009; Siana et al. 2009), we need to observe this type of galaxy at lower redshifts to understand their dust emission. Burgarella et al. (2007) detected dropout galaxies at $z \sim 1$ at 24 μm with *Spitzer*; however, the dust luminosities estimated from the rest-frame 12 μm flux density is far from the peak of the dust emission and could provide biased SFR estimates.

We observe in the FIR a sample of LBGs at $0.7 < z < 1.6$ (FUV dropouts) and at $1.6 < z < 2.8$ (near-UV or NUV dropouts). We use the SPIRE instrument (Griffin et al. 2010) on *Herschel* (Pilbratt et al. 2010) with observations from HerMES (Oliver et al. 2010; S. J. Oliver et al. 2011, in preparation).[24] This is the first opportunity to directly estimate the dust luminosity

[24] http://hermes.sussex.ac.uk

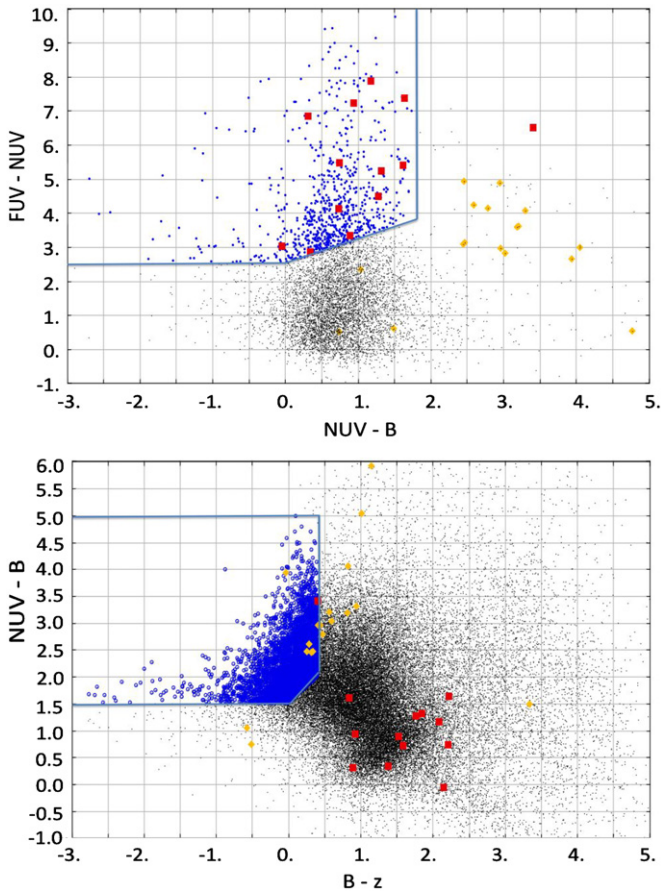

Figure 1. Upper panel shows the selection for $0.7 < z < 1.6$ dropouts: $m[\mathrm{FUV}] - m[\mathrm{NUV}] \geqslant 0.7(m[\mathrm{NUV}] - B) + 2.5$; $m[\mathrm{FUV}] - m[\mathrm{NUV}] \geqslant 2.5$; $m[\mathrm{NUV}] - B \leqslant 1.8$; and S/N(NUV) $\geqslant 3$. This corresponds to 740 objects, with an average S/N(NUV) = 8.6. The lower panel shows the selection for $1.6 < z < 2.8$ dropouts: $m[\mathrm{NUV}] - B \geqslant 1.25(B-z)+1.5$; $m[\mathrm{NUV}] - B \geqslant 1.5$; $m[\mathrm{NUV}] - B \leqslant 5.0$; $B - z \leqslant 0.4$; and S/N(B) $\geqslant 3.0$, which corresponds to 4107 objects, with a sample average S/N(B) = 9.7. The LBGs are shown as blue dots and the SPIRE-detected LBGs by big (red) boxes. Both LBG samples are plotted on each panel. Yellow diamonds are stars.

(A color version of this figure is available in the online journal.)

(or upper limits) of unlensed LBGs from FIR data. We assume $\Omega_{\mathrm{m}} = 0.3$, $\Omega_{\Lambda} = 0.7$, and $H_0 = 71\,\mathrm{km\,s^{-1}\,Mpc^{-1}}$ and use AB magnitudes throughout.

2. DATA

2.1. LBG Samples

Observations of the Great Observatories Origins Deep Survey North (GOODS-N) were secured as part of the *Herschel* Multi-tiered Extragalactic Survey (HerMES; Oliver et al. 2010) by *GALEX* in FUV and NUV. We define two samples of galaxies in two redshift ranges corresponding to FUV dropouts and NUV dropouts (Figure 1).

The photometry. is performed with IRAF DAOPHOT II (Stetson 1987) in the NUV, and in the FUV with the NUV coordinates. Using ADDSTAR, the completeness is estimated to 80% down to $m[\mathrm{FUV}] = 24.9$ and $m[\mathrm{NUV}] = 24.2$. We use CIGALE (Noll et al. 2009) to build models in the range $0 \leqslant z \leqslant 3$ and delimit the regions corresponding to LBGs at $0.7 < z < 1.6$ and $1.6 < z < 2.8$ in the color–color diagrams.[25] The sample is cross-correlated with the R-selected Capak et al. (2004) multiwavelength catalog over 0.4 deg^2, with a search radius of $1''$, producing a catalog of 86,768 entries (46,076 with *GALEX* data, 47,450 with optical data, and 6979 objects with both). The U-band data were collected using the Kitt Peak National Observatory 4 m telescope. The B-, V-, R-, I-, and z-band data were collected using the Subaru 8.2 m telescope and Suprime-Cam instrument with 5σ limiting magnitudes of $U = 27.1$, $B = 26.9$, $V = 26.8$, $R = 26.6$, $I = 25.6$, and $z = 25.4$. Photometric redshifts are computed using Le Phare (Arnouts et al. 2002; Ilbert et al. 2009) and we use them in addition to spectroscopic redshifts from Barger et al. (2008). In the redshift range $0.7 < z < 1.6$, we compare photometric to spectroscopic redshifts (784 galaxies) and find $\sigma_z / (1 + z) = 0.036$ while we have (24 galaxies) $\sigma_z/(1 + z) = 0.125$ at $1.6 < z < 2.8$.

From the lower redshift catalog, 27 objects (4%) have photometric redshifts at $z < 0.7$, 696 objects (94%) are in our redshift range of $0.7 < z < 1.6$, and 17 objects (2.3%) are at $z > 1.6$. For the higher redshift catalog, 223 objects (5%) have photometric redshifts at $z < 1.6$, 3859 objects (94%) are in our redshift range of $1.6 < z < 2.8$, and 25 objects (0.6%) are at $z > 2.8$.

2.2. Matching with SPIRE

We cross-correlate the LBG samples with the HerMES multiwavelength catalog from Roseboom et al. (2010). It uses 24 μm sources as a prior, so we restrict ourselves to the deep GOODS-N MIPS region of $19' \times 12'$, i.e., 0.063 deg^2. Within this region we have 260 low-z LBGs and 1558 high-z. This HerMES catalog contains 1951 24 μm sources as an input to the association process. A search radius of $1''$ is chosen, since the 3.6 μm positions are good to that accuracy. Given the source density of the HerMES catalog, this should return <1% spurious matches. We find 86 matches between this list and our LBG samples, with 63 matches to the low-z sample and 23 matches to the high-z sample, with ~2 (3.2%) and ~11 (47.8%), respectively, expected by chance.

The HerMES catalog gives SPIRE measurements for all MIPS sources. To define confident SPIRE detections, we require flux densities higher than 7.6, 9.2, or 10.4 mJy at 250, 350 and 500 μm respectively. This flux limit corresponds to $2 \times \sigma_{\mathrm{faint}}$, the clipped map confusion noise, where σ_{faint} is estimated by Nguyen et al. (2010) from the map variance after removing pixels brighter than $5\sigma_{\mathrm{conf}}$ (the raw map confusion noise). Imposing these more reasonable flux density limits gives 14 low-z candidates and one high-z candidate.

We define SPIRE detections (listed in Table 1) whenever the signal-to-noise ratio (S/N) is larger than 3 and their "purity" index (see Roseboom et al. 2010; Brisbin et al. 2010) is larger than 0.2. Note that according to this definition there are no detections at 500 μm. The "purity" of the SPIRE flux density is estimated from the ratio of this source's 24 μm flux density to the 24 μm one smoothed with the SPIRE beam at this position. For no "pollution," the purity is 1 and decreases when there are possible contributions by other sources. We additionally inspected the images around each candidate to check for contamination by neighbors. Based on the purity index, we exclude two objects at $0.7 < z < 1.6$. All but one of the sources on the final sample (actually the highest redshift LBG) have S/N $\gtrsim 6$ (see Table 1).

The final $0.7 < z < 1.6$ HerMES LBG sample contains 12 objects and the $1.6 < z < 2.8$ sample contains one object. Although it is difficult to determine what fraction of

[25] Note that the code accounts for intergalactic medium attenuation

Table 1
Observational Data and Physical Parameters Deduced by CIGALE

ID	z	Origin Redshift	m[NUV] (AB)	U (AB)	S_{24} (μJy)	S_{250} (mJy)	S_{350} (mJy)	$S_{1.4\,\mathrm{GHz}}$ (mJy)	$\log M_*$ ($M_\odot$)	SFR ($M_\odot$ yr^{-1})	$\log L_{\mathrm{IR}}$ ($M_\odot$)	A_{FUV} (mag)	$\log L_{\mathrm{FUV}}$ ($L_\odot$)	T_{d} (K)
J123624.6+620610.2	0.75	0.11	22.87 ± 0.04	23.25 ± 0.04	93.2 ± 8.3	8.0 ± 0.9	···	···	10.0 ± 0.1	23.5 ± 0.048	11.1 ± 0.039	1.96 ± 0.14	10.4 ± 0.6	···
J123547.4+621005.9	0.81	0.24	24.07 ± 0.07	25.33 ± 0.24	86.3 ± 7.6	11.3 ± 0.9	12.1 ± 1.5	···	10.2 ± 0.1	34.8 ± 0.030	11.3 ± 0.007	3.68 ± 0.28	9.9 ± 1.4	···
J123724.8+620938.5	0.81	0.13	22.80 ± 0.04	23.59 ± 0.06	249.0 ± 6.7	10.3 ± 0.8	···	···	10.7 ± 0.1	39.4 ± 0.090	11.3 ± 0.094	2.42 ± 0.28	10.5 ± 0.9	···
J123633.2+620834.9	0.93	specz	22.41 ± 0.03	22.84 ± 0.03	779.0 ± 7.9	22.4 ± 1.2	19.2 ± 1.8	50.8 ± 10.2	11.1 ± 0.2	119.7 ± 0.040	11.9 ± 0.027	2.84 ± 0.18	10.9 ± 1.1	24.3
J123714.4+622112.3	0.94	specz	24.20 ± 0.08	25.17 ± 0.21	212.0 ± 4.6	9.2 ± 1.2	12.0 ± 2.7	···	10.7 ± 0.2	43.9 ± 0.059	11.4 ± 0.050	3.46 ± 0.32	10.1 ± 1.3	···
J123624.4+620836.3	0.95	specz	23.22 ± 0.05	23.83 ± 0.07	695.0 ± 11.5	21.1 ± 2.8	22.9 ± 7.0	···	11.3 ± 0.2	116.4 ± 0.182	11.9 ± 0.156	3.45 ± 0.50	10.6 ± 1.3	24.2
J123614.4+620718.5	0.97	specz	23.88 ± 0.07	25.32 ± 0.23	386.0 ± 8.7	9.2 ± 1.0	10.2 ± 1.2	···	11.0 ± 0.2	61.8 ± 0.275	11.7 ± 0.218	3.52 ± 0.78	10.3 ± 1.4	···
J123721.4+621346.1	1.02	specz	24.53 ± 0.10	24.41 ± 0.11	235.0 ± 7.5	15.4 ± 2.6	···	41.6 ± 8.7	11.0 ± 0.2	113.2 ± 0.134	11.9 ± 0.120	4.52 ± 0.38	10.2 ± 1.7	···
J123618.6+621115.2	1.02	specz	21.79 ± 0.03	23.40 ± 0.05	404.0 ± 5.4	14.5 ± 2.3	···	36.5 ± 11.1	11.3 ± 0.2	135.5 ± 0.161	11.9 ± 0.133	2.60 ± 0.42	11.0 ± 0.9	···
J123722.5+621356.6	1.02	specz	23.46 ± 0.06	24.78 ± 0.15	317.0 ± 6.2	9.7 ± 1.2	11.5 ± 2.3	23.7 ± 4.7	10.9 ± 0.2	74.0 ± 0.155	11.7 ± 0.145	3.23 ± 0.43	10.4 ± 1.2	···
J123808.9+621847.5	1.04	0.29	22.89 ± 0.06	23.66 ± 0.06	218.0 ± 8.8	9.8 ± 1.1	···	···	10.8 ± 0.3	78.2 ± 0.168	11.6 ± 0.156	2.46 ± 0.40	10.8 ± 0.8	···
J123709.0+622318.5	1.33	0.28	22.91 ± 0.05	23.91 ± 0.08	247.0 ± 6.7	28.2 ± 1.3	14.3 ± 2.4	176.4 ± 13.9	11.2 ± 0.1	448.8 ± 0.066	12.4 ± 0.027	3.82 ± 0.18	11.1 ± 1.3	51.8
J123629.6+620901.2	1.97	0.67	24.33 ± 0.09	···	110.0 ± 6.0	···	10.5 ± 2.4	···	10.5 ± 0.1	893.3 ± 0.036	12.5 ± 0.035	4.30 ± 0.20	11.1 ± 1.5	···

Note. The column origin redshift is "specz" if the redshift is spectroscopic or the 3σ uncertainty otherwise.

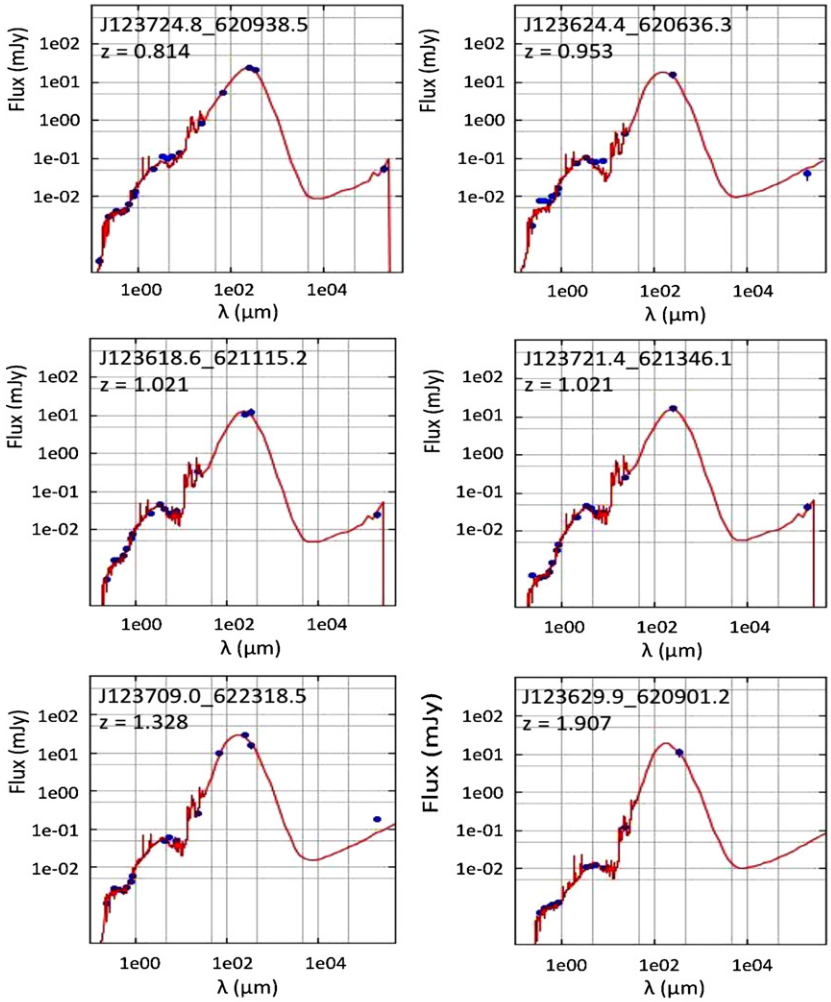

Figure 2. Observed spectral energy distributions of LBGs superimposed on best-fit models (S_ν[mJy] vs. log λ[μm]). Note that J123633.2 + 620834.9 very likely hosts an AGN, as suggested by the CIGALE SED fitting.

(A color version of this figure is available in the online journal.)

$z \sim 2$ LBGs should be detected in the FIR, we can use the *Spitzer* 24 μm data to estimate how many $z \sim 1$ LBGs are expected to be detected at 250 μm. From the present sample, the mean ratio $S_{250}/S_{24} = 54 \pm 11$ for the SPIRE-detected LBGs and so, the present 250 μm detection limit of 7.6 mJy correspond to 140 μJy at 24 μm. At this level, and based on the 24 μm catalog, we would expect 20 $z \sim 1$ LBGs to be detected with SPIRE at 250 μm. We find 12 objects, i.e., 60% of the expectation. This is consistent with the completeness at this flux level in Roseboom et al. (2010).

2.3. SED Fitting

Dust luminosities ($L_{\rm IR} = L[8-1000\,\mu{\rm m}]$) and other parameters are estimated using CIGALE (Noll et al. 2009).[26] CIGALE performs a Bayesian analysis to estimate parameter by fitting models to the UV-to-submillimeter spectral energy distributions (SEDs). One can select among two single stellar population libraries and several IR models/templates. An active galactic nucleus (AGN) component can also be added to estimate the AGN fraction (contribution by a potential AGN to $L_{\rm IR}$). The parameters of the dust attenuation law can be modified and CIGALE allows for two separate stellar populations with a multiphase dust treatment.

We use the Very Large Array 1.4 GHz radio data from Morrison et al. (2010) which provides data down to an rms noise of 3.9 μJy per beam. The stellar emission is based on Maraston (2005), while the dust emission is based on Dale & Helou (2002) templates. CIGALE provides dust luminosities $L_{\rm IR}$, while FUV luminosities $L_{\rm FUV}$ are derived at $\lambda_{\rm rest} = 153$ nm and are defined through the quantity νL_ν. An energy budget is performed during the fit, and the maximum value allowed for $L_{\rm IR}$ has to be consistent with the energy moved by dust grains from the UV-optical range to the FIR range.

Individual SEDs with the best models selected by CIGALE are shown in Figure 2 for the five LBGs with radio data and for the $z = 1.9$ LBG. Observational and physical parameters are given in Table 1. Figure 2 shows that CIGALE is able to fit the SEDs from the FUV to the radio successfully. The average FUV luminosity of the SPIRE detected objects is $\log\langle L_{\rm FUV}/L_\odot\rangle = 10.7 \pm 0.2$, and most of them are therefore UV-luminous galaxies. Their average dust luminosity is $\log\langle L_{\rm IR}/L_\odot\rangle = 11.9 \pm 0.1$ and their stellar average mass is $\log\langle M_*/M_\odot\rangle = 11.0 \pm 0.5$. A comparison with Magdis et al. (2010) shows that the average stellar mass is similar to the average stellar mass

[26] http://www.oamp.fr/cigale

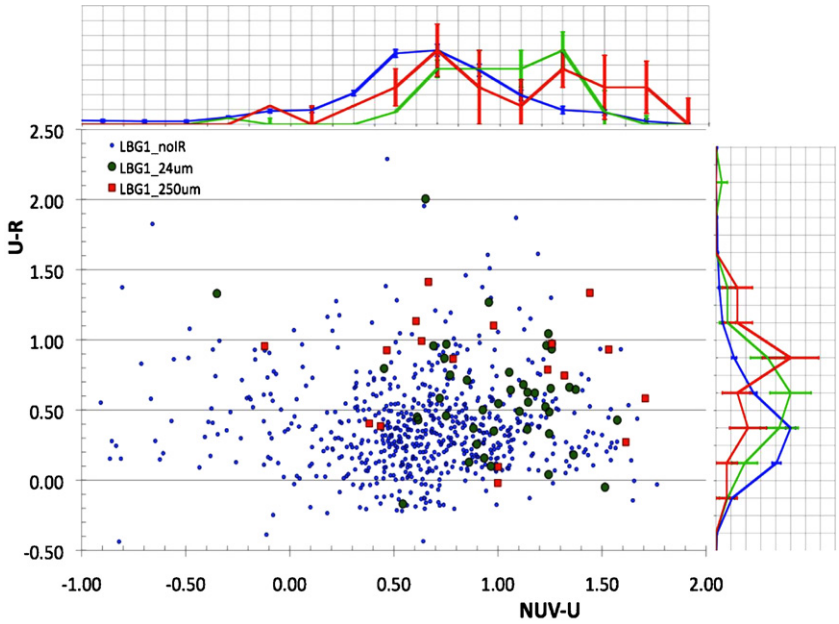

Figure 3. In this ($U - R$) vs. (m[NUV] $- U$) diagram, blue points are LBGs which are undetected at 24 μm, green dots are those detected at 24 μm, and red boxes are those detected in the FIR with *Herschel*. We see on the marginal distributions that LBGs get redder with increasing maximum wavelength of detection, especially in the $U - R$ color. This is expected if IR-bright LBGs are more attenuated than IR-faint LBGs.

(A color version of this figure is available in the online journal.)

($\log\langle M_*/M_\odot\rangle = 11$) of $z \sim 3$ LBGs detected at $\lambda = 8\,\mu$m. The dust temperatures T_d are estimated for a few objects by fitting modified blackbodies with an emissivity index of 1.5. We find that two of the low-z LBGs have $T_d \sim 24$ K, while the high-z ULIRG has $T_d = 52$ K (see Table 1). The two low-z LBGs have quite low temperatures compared with ULIRGs/SMGs, but may be typical of star-forming galaxies in general, while the high-z one is similar to, e.g., Arp220.

3. DUST ATTENUATION OF LYMAN BREAK GALAXIES

Our LBG SEDs in the rest-frame UV are in very good agreement with the rest-frame UV spectra of the Shapley et al.'s (2003) composite spectrum at $z \sim 3$. Whatever the redshift range, LBGs seem to present the same starburst characteristics in the rest-frame UV, which is expected, given that similar rest-frame color selection criteria are used. However, the colors become redder when the objects are detected at 24 μm by *Spitzer* and even redder when they are detected at 250 μm by *Herschel* SPIRE. This can be interpreted as being due to higher dust attenuations (see Figure 3), and is consistent with Burgarella et al. (2007), who found that both *Spitzer*-detected and undetected LBGs have about the same stellar population ages, but the latter are more extinguished.

The AGN fraction determined by CIGALE is always consistent with zero, except for the galaxy J123633.2+620834.3, for which a 20% AGN contribution to the FIR dust luminosity is suggested. Most of the IR excess due to a potential AGN should be in the MIR, while the SPIRE flux is expected to be dominated by the starburst component (Hatziminaoglou et al. 2010); CIGALE accounts for both.

The vast majority of the dropout galaxies are not detected by SPIRE with the present detection limits. If LBGs were to follow Meurer et al. (1999) relation (relating UV attenuation to dust emission), what fraction of them would be detectable? We can use the ($U - V$) color as a proxy for the rest-frame m[FUV]$-m$[NUV]. Simulations suggest that this color provides β with an accuracy better than 0.01 for power laws $f_\lambda \propto \lambda^\beta$ and $\beta = -2, -1$, and 0. In detail, we can estimate

$$\begin{aligned}\beta &= \log[f_\nu(\mathrm{FUV})/f_\nu(\mathrm{NUV})]/\log[\lambda_{\mathrm{FUV}}/\lambda_{\mathrm{NUV}}] - 2.00\\ &= 5.39\log[S_\nu(\mathrm{FUV})/S_\nu(\mathrm{NUV})] - 2.00. \qquad (1)\end{aligned}$$

From the β values, we estimate $\log(L_{\mathrm{IR}}/L_{\mathrm{FUV}})$ for the LBGs and, after evaluating L_{FUV} from the filter closest to $\lambda_{\mathrm{FUV}} = 0.15$ nm (as a function of the redshift), we determine L_{IR}. These values of L_{IR} can be transformed into L_{250} and S_{250} using the following calibrations computed from the Dale & Helou (2002) models with $1.0 \leqslant \alpha \leqslant 2.5$, i.e., star-forming galaxies with similar properties to LBGs. We have also checked that Chary & Elbaz (2001) models are consistent with our calibration. By fitting polynomials as a function of redshift, we find

$$\log L_{\mathrm{IR}} = \sum_{i=0}^{3} C_i z^i + \log(\nu L_\nu)\,|_\lambda\ , \qquad (2)$$

with $C \equiv (C_0, C_1, C_2, C_3) = (1.168, -1.166, 0.565, -0.091)$ for $\lambda = 250\,\mu$m, $(1.689, -1.426, 0.582, -0.089)$ for $\lambda = 350\,\mu$m, and $(2.336, -1.605, 0.556, -0.078)$ for $\lambda = 500\,\mu$m.

Assuming the Meurer et al. (1999) relation allows to estimate rough order of magnitude $L_{\mathrm{IR}}/L_{\mathrm{FUV}}$ for our LBGs (Burgarella et al. 2009). At 250 μm we should have detected 10 LBGs from the sample undetected in the mid-IR and far-IR, three LBGs from those detected at 24 μm, and two LBGs from those detected at 250 μm.

For the LBGs not detected by *Herschel*, we can estimate upper limits of $\log(L_{\mathrm{IR}})$ for each SPIRE band and we use the lowest of the three values as the final upper limit on $L_{\mathrm{IR}}/L_{\mathrm{FUV}}$. From $\log(L_{\mathrm{IR}}/L_{\mathrm{FUV}})$ we can estimate A_{FUV}. Figure 4 suggests that the maximum level of attenuation depends on L_{FUV}—the most UV-luminous LBGs yield a lower maximum A_{FUV} than less UV-luminous ones. This is true for upper limits as well as for detections. The two higher redshift lensed LBGs detected in

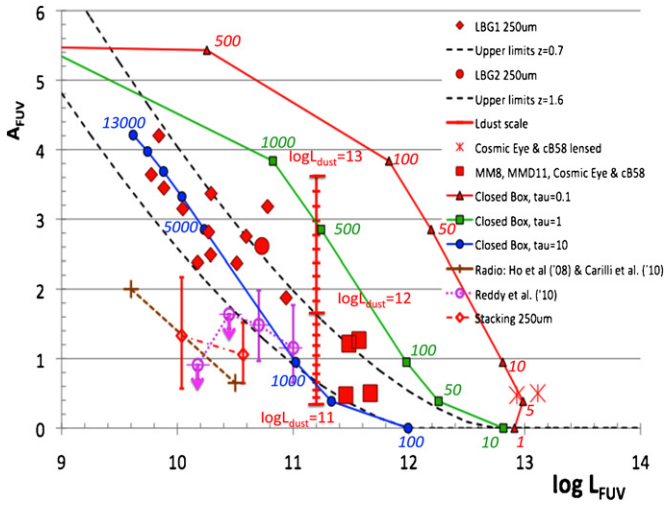

Figure 4. Red diamonds are LBGs detected by *Herschel*. The two big red stars are the two high-redshift LBGs (the Cosmic Eye and cB58) as observed, while the big red squares are the same sources after correcting for the amplification plus two unlensed ones. The blue dots, green boxes, and red triangles are the closed-box models, plotted as a function of time (age in Myr) increasing from the bottom right to the top left part of the diagram. All the models would scale to the left with decreasing mass. The vertical scale provides the values of $L_{\rm IR}$ in steps of 0.1 dex. The two crosses linked by a dashed line are radio-based measurements. The purple open dots are the stacked points from Reddy et al. (2010). The red open diamonds correspond to stacked points at $z \sim 1$ from our sample. The bottom line of this figure is that the maximum dust attenuation appears to decline with increasing $L_{\rm dust}$.

(A color version of this figure is available in the online journal.)

FIR or in submillimeter (the "Cosmic Eye," Siana et al. 2009; cB58, Siana et al. 2008) also comply with this upper boundary, if we correct for the amplification. As do the two unlensed LBGs MM8 (Chapman et al. 2000) and MMD11 (Chapman & Casey 2009). We stress that most of the upper limits should populate the area below the observational limits but none would prevent us from detecting LBGs that would have larger FUV dust attenuations than the one suggested by the present data for a given $L_{\rm FUV}$.

Reddy et al. (2010) suggest that objects with a lower UV luminosity at $1.5 \leqslant z \leqslant 2.6$ have lower bolometric luminosities than UV-bright galaxies which, in turn, may suggest lower dust attenuations if we account for the relation between bolometric luminosities and dust attenuations. This is in agreement with Bouwens et al. (2010) at much higher redshifts. But, when computing $A_{\rm FUV}$ from the stacked points of Reddy et al. (2010), we find a trend similar to ours for most of the points. Carilli et al. (2008) and Ho et al. (2010) estimate the UV dust attenuation by comparing radio-based star formation rates to UV-based ones using a stacking analysis. We show in Figure 4 the two points corresponding to different log $L_{\rm FUV}$ and they agree with the above trend. Burgarella et al. (2006) reached a similar conclusion using *Spitzer* 24 μm observations of a sample of LBG at $z \sim 1$. Finally, we have divided our $z \sim 1$ sample in two sub-samples as a function of $L_{\rm FUV}$ and stacked them in the 250 μm image (Figure 4). We find the same trend again. Note, however, that accounting for the error bars, our stacking and Reddy et al.'s (2010), are both consistent with a constant $A_{\rm FUV}$. Also, whenever the selection is not fully complete, one may miss objects in the regions where the brightest sources (UV and IR) lie. This effect due to the inhomogeneous background produces holes in the stacking (see, e.g., Bavouzet 2008). For this very reason, the $z \sim 1$ stacked points are only considered as lower limits and we were not able to stack $z \sim 2$ LBGs.

To understand the origin of this effect, we build a simple closed-box model (see Pagel 1997), assuming several exponentially decreasing star formation histories $\Psi(t) = \Psi_0 e^{-t/\tau}$, with $\tau = 0.1$, 1, and 10 Gyr. We assume a mass of cold gas $M_{\rm gas}$ that forms stars following a Salpeter initial mass function, and thus produce heavy elements. $M_{\rm gas}$ evolves as follows:

$$dM_{\rm gas}/dt = -\Psi(t) + E(t), \quad (3)$$

where $E(t)$ is the mass ejected by stars at the end of their lifetime.

The oxygen abundance $z_{\rm O}$ can be estimated as

$$Z_{\rm O} = -p_{\rm O} \ln[1 - \alpha(1 - e^{-t/\tau})], \quad (4)$$

where $p_{\rm O}$ is the oxygen yield and α is the fraction of mass kept in stellar remnants. We estimate an empirical relation from Reddy et al. (2010) that links $12 + \log({\rm O/H})$ to $L_{\rm IR}$:

$$\log(L_{\rm IR}/L_{\rm FUV}) = 1.67(12 + \log({\rm O/H})) - 12.72. \quad (5)$$

Reddy et al.'s (2010) objects are in the redshift range $1.5 \leqslant z \leqslant 2.6$, so very close to ours and with metallicities in the range $8.2 < 12/\log({\rm O/H}) < 8.8$ which corresponds to ages in the range of a few 100 Myr to 5 Gyr. So, strictly speaking, our models are extrapolations for low τs but are in the good range for $\tau = 10$ Gyr. Finally, from $L_{\rm IR}$ we compute $A_{\rm FUV}$ using the relationship from Burgarella et al. (2005).

Figure 4 shows that this simple closed-box model follows the same trend as our LBGs in the diagram. The initial mass of gas is set to $\log(M_{\rm gas}/M_\odot) = 10.5$ to explain the low-redshift LBGs and $\log(M_{\rm gas}/M_\odot) = 11.0$ (not plotted) for the high-redshift LBGs. This is in agreement with the mass of cold gas predicted by models (e.g., Lacey et al. 2011). We find that star formation timescales of $\tau \lesssim 1$ Gyr seem to be ruled out by this model.

4. CONCLUSIONS

We have selected two samples of LBGs at $z \sim 1$ and $z \sim 2$. For the first time, we can put constraints on the dust emission and therefore the dust attenuation of LBGs directly from rest-frame FIR measurements of individual LBGs observed with *Herschel*-SPIRE. Two main conclusions can be drawn from this analysis.

We detected $12/260 \sim 4.6\%$ and $1/1558 \sim 0.06\%$ of the LBGs at $0.7 \leqslant z \leqslant 1.6$ and $1.6 \leqslant z \leqslant 2.8$, respectively. All the other LBGs are undetected by SPIRE, and their dust attenuation is lower than the detected LBGs. However, we have to account for the fact that the limits depend on $L_{\rm FUV}$.

Second, the maximum dust attenuation in the FUV decreases as UV luminosities increase.

Other points of interests are as follows.

1. The dropout selections presented in this paper are very efficient (~95%) at detecting galaxies in the redshift range $0.7 \leqslant z \leqslant 2.8$.
2. The rest-frame UV SEDs of the two dropout samples are similar to higher redshift LBGs.
3. CIGALE is able to model the observed SEDs from the FUV to the radio and we provide the derived physical parameters.
4. The stellar masses of these IR-bright dropout galaxies are of the same order as the stellar masses of IR-bright LBGs observed in IRAC and MIPS bands.

5. We propose that all LBGs lie in a triangle-shaped region in the $A_{\rm FUV}$ versus $\log L_{\rm FUV} = 0$ diagram limited by dust-free (small and/or young) galaxies to the bottom and by the locus for evolving most massive galaxies to the top.

SPIRE has been developed by a consortium of institutes led by Cardiff University (UK) and including University of Lethbridge (Canada); NAOC (China); CEA, OAMP (France); IFSI, University of Padua (Italy); IAC (Spain); Stockholm Observatory (Sweden); Imperial College London, RAL, UCL-MSSL, UKATC, University of Sussex (UK); and Caltech/JPL, IPAC, University of Colorado (USA). This development has been supported by national funding agencies: CSA (Canada); NAOC (China); CEA, CNES, CNRS (France); ASI (Italy); MCINN (Spain); Stockholm Observatory (Sweden); STFC (UK); and NASA (USA). The data presented in this paper will be released through the *Herschel* Database in Marseille (HeDaM; http://hedam.oamp.fr/HerMES). This work makes use of TOPCAT (http://www.star.bristol.ac.uk/∼mbt/topcat/).

REFERENCES

Arnouts, S., Moscardini, L., Vanzella, E., Colombi, S., Fontana, A., Giallongo, E., Matarrese, S., & Saracco, P. 2002, MNRAS, 329, 355
Barger, A. J., Cowie, L. L., & Wang, W.-H. 2008, ApJ, 689, 687
Bavouzet, N. 2008, PhD Thesis, Univ. Paris (http://tel.archives-ouvertes.fr/index.php?halsid=h876uaf6oo0uo8vm9ui00brvn6&view_this_doc=tel-00363975&version=1)
Bouwens, R. J., et al. 2010, ApJ, 708, 69
Brisbin, D. the HerMES Consortium. 2010, MNRAS, 409, 66
Buat, V., & Xu, C. 1996, A&A, 306, 61
Burgarella, D., Buat, V., & Iglesias-Páramo, J. 2005, MNRAS, 360, 1413
Burgarella, D., Buat, V., Takeuchi, T. T., Wada, T., & Pearson, C. 2009, PASJ, 61, 177
Burgarella, D., Le Floc'h, E., & Takeuchi, T. T. 2007, MNRAS, 380, 986
Burgarella, D., et al. 2006, A&A, 450, 69
Capak, P., et al. 2004, AJ, 127, 180
Carilli, C. L., et al. 2008, ApJ, 689, 883
Chapman, S. C., & Casey, C. M. 2009, MNRAS, 398, 1615
Chapman, S. C., et al. 2000, MNRAS, 319, 318
Chary, R., & Elbaz, D. 2001, ApJ, 556, 562
Dale, D. A., & Helou, G. 2002, ApJ, 576, 159
Griffin, M., et al. 2010, A&A, 518, L3
Hatziminaoglou, E., et al. 2010, A&A, 518, L33
Ho, I. T., Wang, W.-H., Morrison, G. E., & Miller, N. A. 2010, ApJ, 722, 1051
Ilbert, O., et al. 2009, ApJ, 690, 1236
Lacey, C. G., Baugh, C. M., Frenk, C. S., & Benson, A. J. 2011, MNRAS, 412, 1828
Magdis, G. E., Elbaz, D., Daddi, E., Morrison, G. E., Dickinson, M., Rigopoulou, D., Gobat, R., & Hwang, H. S. 2010, ApJ, 714, 1740
Maraston, C. 2005, MNRAS, 362, 799
Meurer, G. R., Heckman, T. M., & Calzetti, D. 1999, ApJ, 521, 64
Morrison, G. E., Owen, F. N., Dickinson, M., Ivison, R. J., & Ibar, E. 2010, ApJS, 188, 178
Nguyen, H. T., et al. 2010, A&A, 518, L5
Noll, S., Burgarella, D., Giovannoli, E., Buat, V., Marcillac, D., & Muñoz-Mateos, J. C. 2009, A&A, 507, 1793
Oliver, S. J., et al. 2010, A&A, 518, L21
Pagel, B. E. J. 1997, Nucleosynthesis and Chemical Evolution of Galaxies (Cambridge: Cambridge Univ. Press)
Pilbratt, G. L., et al. 2010, A&A, 518, L1
Reddy, N. A., Erb, D. K., Pettini, M., Steidel, C. C., & Shapley, A. E. 2010, ApJ, 712, 1070
Roseboom, I., et al. 2010, MNRAS, 409, 48
Shapley, A. E., Steidel, C. C., Pettini, M., & Adelberger, K. L. 2003, ApJ, 588, 65
Siana, B., Teplitz, H. I., Chary, R.-R., Colbert, J., & Frayer, D. T. 2008, ApJ, 689, 59
Siana, B., et al. 2009, ApJ, 698, 1273
Stetson, P. B. 1987, PASP, 99, 191